Running title: Natural nanoparticle evolution in paddy soils

Changes in profile distribution and chemical properties of natural nanoparticles as affected by rice cultivation

Dan HUANG[a,b], Xinyu ZHU[a,b], Baile XU[a,b], Yan HE[a,b], Mingkui ZHANG[a,b], Fei LIU[a,b], Zhenghua LIAN[a,b], Randy A. DAHLGREN[c], Philip C. BROOKES[a,b], Jianming XU[a,b,*]

[a] Institute of Soil and Water Resources and Environmental Science, College of Environmental and Resource Sciences, Zhejiang University, Hangzhou 310058, China
[b] Zhejiang Provincial Key Laboratory of Agricultural Resources and Environment, Hangzhou 310058, China
[c] Department of Land, Air and Water Resources, University of California – Davis, Davis, CA 95616, USA

*Corresponding author. Tel/fax: +86-571-88982069.
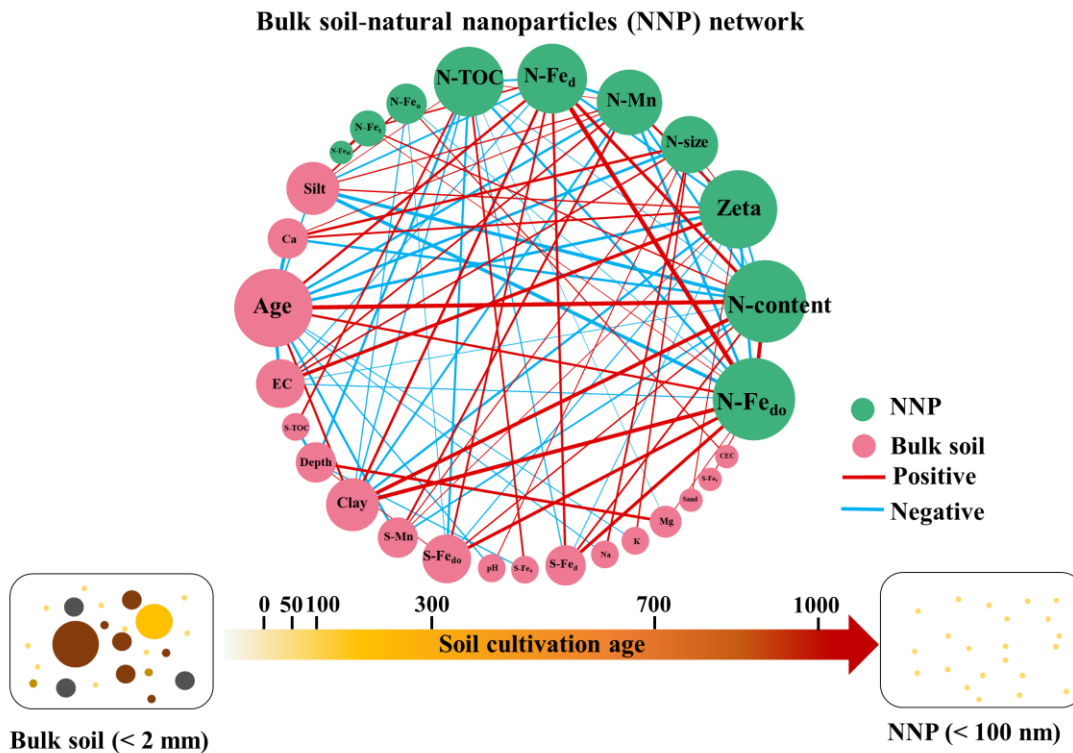*E-mail address:* jmxu@zju.edu.cn.
Institute of Soil and Water Resources and Environmental Science, College of Environmental and Resource Sciences, Zhejiang University, 866 Yuhangtang Road, Hangzhou 310058, China.

ABSTRACT

Systematic studies of the genesis, properties and distribution of natural nanoparticles (NNPs) remain scarce in soil environments. This study examines a soil chronosequence having continuous rice paddy land use for periods ranging from 0 to 1000 years to determine how the NNP fraction changes during the early stages of soil genesis in eastern China. Samples were collected from coastal reclaimed soils that were cultivated for 0, 50, 100, 300, 700 and 1000 years. The NNP fraction was isolated and characterized along with bulk soil samples (< 2-mm fraction) for selected physical and chemical properties. NNP content increased with increasing cultivation age (6.0 kg m^{-2} 100 yr^{-1}). It was related to the reduction in electrical conductivity (EC) (172−1297 μS cm^{-1}) and NNP zeta potentials [−(22−36 mV)] with the increasing age. Changes in several NNP properties, such as pedogenic Fe and total organic carbon (TOC), were consistent with those occurring in the bulk soil fraction across the chronosequence. Notably, changes in Fe fractions were obvious and illustrated active chemical weathering, pedogenesis and potential impacts on the microbial community. Redundancy analysis demonstrated that soil cultivation age was the most important factor affecting NNP properties, contributing 60.7% of the total variation. After an initial period of desalinization (~50 yrs), cluster and principal component analysis (PCA) revealed that NNP samples split into age groups of 50−300 yrs and 700−1000yrs indicating rapid evolution of NNP properties. Overall, this study provides new insights for NNP evolution during pedogenesis and for predicting their influences on agriculture and ecological risks over millennial-scale rice cultivation.

GRAPHICAL ABSTRACT

INTRODUCTION

Natural nanoparticles (NNPs), defined as naturally-produced particles having one dimension < 100 nm, are ubiquitous and display a variety of chemical and mineralogical compositions (Hochella *et al.*, 2008; Li *et al.*, 2012; Zhu *et al.*, 2017). The annual production of NNPs originated from biogeochemical processes is estimated to be several thousands of teragrams (1 Tg = 1 million metric tons) (Hochella *et al.*, 2015). The NNP soil fraction has a disproportionate importance relative to its abundance with respect to several crucial ecological services (Theng and Yuan, 2008; Hochella *et al.*, 2019), including influencing soil hydrological properties (Zhang *et al.*, 2016), long-distance translocation of soil particles (Rod *et al.*, 2018), and sorption and transport of contaminants and nutrients in the subsurface environment (Bakshi *et al.*, 2015; Taghipour and Jalali, 2018; Liu *et al.*, 2019a). These widely distributed soil particles, including mineral weathering products and organic particles derived from the decay of plant and microbial debris, have a complex composition that is affected by soil formation pathways (Li *et al.*, 2012; Van Den Bogaert *et al.*, 2015). The recent

development of enhanced NNP extraction and characterization methods provides a strong foundation for further studies of NNPs (Bakshi *et al.*, 2014; Liu *et al.*, 2019a).

At the nano-scale (1–100 nm), NNP properties may be very different from soil colloids (Taghipour and Jalali, 2018). Our previous study demonstrated that soil NNPs had a higher mobility than the clay fraction (Liu *et al.*, 2018). Moreover, NNPs act as carriers for contaminants and thus likely facilitate the spread of contaminants, posing a potential risk to groundwater (Liu *et al.*, 2019a; Wang *et al.*, 2019; Xu *et al.*, 2019). Thus, it is important to study soil physical and chemical properties across a wide range of spatial and temporal scales to better understand soil physio-chemical processes resulting in NNP formation (Hochella *et al.*, 2019). Given the high reactivity of NNPs, they play a disproportionate role and therefore require special attention, especially regarding their fate and transport over pedogenic time scales.

As the dominant agricultural soils worldwide, paddy soils occupy 11% (1 956 000 km^2) of the cultivated land area and provide a fundamental food source (Leff *et al.*, 2004; Song *et al.*, 2017). Paddy soils have complex redox conditions and variations in organic matter during rice cultivation processes (Jiang *et al.*, 2017), which likely make the NNP distribution and properties different from other soils. However, the properties, fate and environmental influence of NNPs in paddy soils have received little study, thereby warranting further investigation.

Soil physical and biogeochemical properties are particularly dynamic in paddy soils due to long-term, managed oxidation and reduction cycles. Previous studies have mainly focused on organic carbon dynamics (Wei *et al.*, 2018), greenhouse gas emissions (*e.g.,* CO_2, CH_4, N_2O) (Zhu *et al.*, 2018; Liu *et al.*, 2019b; Qian *et al.*, 2020) and soil microbial properties (Watanabe *et al.*, 2020). In addition, puddling of paddy soils strongly influences soil structure characteristics (Zhou *et al.*, 2016) with structure destruction reducing infiltration, which can increase surface runoff and loss of NNPs with associated contaminants (Zhang and Gong, 2003). While some studies have examined clay mineralogy in response to paddy soil management (Wissing *et al.*, 2014; Han *et al.*, 2015), no previous studies have investigated NNP dynamics over long time periods (up to 1000 years) using a well-constrained soil chronosequence approach (Huang *et al.*, 2015). Long-term studies of NNPs provide novel insights for understanding NNP genesis, transformations, and changes of properties in response to long-term paddy management.

Therefore, a paddy soil chronosequence in a coastal area of eastern China, where soils were created by the reclamation of alluvial-marine sediments over the millennial time scale (0 to 1000 years), was established for investigation. Based on bulk soil and NNP characteristics over the 1000-year-long period, we sought to address the following three hypotheses: (1) the distribution and properties of NNPs vary under long-term paddy soil management; (2) the NNP properties are related to changes of bulk soil properties over time; and (3) soil cultivation age and depth are the dominant factors controlling variations in NNP properties. Our main objective was to identify how the abundance and characteristics of paddy soil NNPs changed during long-term (1,000 yrs) rice cultivation.

MATERIALS AND METHODS
Study sites and sample collection

The study was conducted in the coastal area of Cixi on the southern bank of Hangzhou Bay, Zhejiang Province, eastern China (Fig. S1). The area has a typical subtropical monsoon climate with mean annual precipitation of 1325 mm and mean annual temperature of 16.3℃ (Liu *et al.*, 2019c).

The Qiantang River flows downstream to Hangzhou Bay and the East China Sea with an average flow of ~1050 m^3 s^{-1} and mean sediment transport of 212 kg s^{-1} (Guo *et al.*, 2012). Sediment input from the Yangtze River to the north also affects the sedimentation of Hangzhou Bay (Xie *et al.*, 2009, 2017); the dominant clay mineral of the sediment/soil is illite (Wissing *et al.*, 2014). Over the last thousand years, land reclamation has contributed to growth of tidal flats at an average rate of 20 m yr^{-1} (Xie *et al.*, 2009). Dikes were built in different periods to protect the newly developed lands from the tide. Local records accurately document the building of individual dikes allowing us to select sites representing a soil chronosequence (Chen *et al.*, 2011). We selected sites that were cultivated for 0, 50, 100, 300, 700 and 1000 years (Table SI). The 0-year site was a wetland covered with weeds and reeds, while all other sites were paddy fields used for long-term rice cultivation.

For each cultivation age (time since start of paddy management), triplicate soil samples from various depths were collected within a plot of 100−200 m^2. Each profile was divided into five depth increments: 0−20, 20−40, 40−60, 60−80 and 80−100 cm. In the newly developed 0-year wetland, the profile was shallow and only the 0−20 cm depth was collected. All soil samples were air-dried, gently crushed, sieved to < 2 mm and stored for subsequent analyses.

Characterization of soils

Selected soil properties were analyzed following protocols from the National Standards of China (Li *et al.*, 2012); specific methods provided in Table SII of Supplementary Information (SI). After removal of organic matter and total free Fe oxides (Fe_d), the mineral composition of the clay fraction (< 2 μm) was determined by XRD analysis (detailed procedures are presented in SI). Based on the identified soil properties, soils were classified as Fluvaquentic Endoaquolls (Soil Survey Staff, 2014).

Extraction of natural nanoparticles

We used ultrasonic dispersion and centrifugation to isolate NNPs from soil samples following previously established methods (Li *et al.*, 2012; Bakshi *et al.*, 2014). An Ultrasonic Processor VCX750 (Sonics, Newtown, CT, USA) was used to disperse NNP samples at an energy level of 60,000 J. A 3-g soil sample was added to 80 mL deionized water and sonicated for 30 min at a temperature less than 25°C. To reflect the potential for natural mobilization of NNPs, no chemicals were added to assist dispersion. After ultrasonic dispersion, the suspension was passed through a 50-μm sieve and centrifuged (Sorvall ST16R) (Thermo, Osterode, Germany) three times at 3500 *g* for 24 min to collect NNPs (Li *et al.*, 2012). The entire extraction process (ultrasonic dispersion and centrifugation) was repeated 10 times to collect sufficient NNP mass for subsequent analyses. After centrifugation, we collected supernatants in 100-mL glass bottles for particle size and zeta potential analyses. NNP extraction was achieved from all soils, except for the wetland soil (0-yr cultivation) that yielded virtually no NNP particles. Dynamic light scattering (ZetaSizer Nano ZS90, Malvern, Worcestershire, UK) revealed no aggregation of the extracted NNPs.

Characterization of natural nanoparticles

After collection of NNPs, we immediately measured their hydrodynamic size in triplicate using dynamic light scattering in disposable sizing cuvettes (DTS0012) (Sarstedt, Nümbrecht, Germany). Zeta potential was measured at 25°C using a ZetaSizer Nano ZS90 equipped with zeta cells (DTS1060c). Samples were equilibrated for 120 s and zeta potential measurements were repeated in triplicate.

We used transmission electron microscopy (TEM) to examine the size and morphology of NNPs. An aliquot of NNP suspension was placed on a 230-mesh copper film (ZJKY Technology, Beijing, China) and air-dried prior to imaging with a JEOL-JEM-1230 TEM (JEOL, Tokyo, Japan) at 100 kV.

We characterized the mineralogical composition of the NNP fraction using a Bruker D8 Advance XRD (Bruker AXS, Madison, WI).

NNP samples were weighed after drying at 40°C for 24 hours. The elemental composition of the NNP fraction (Fe_t, Mn_t, Al_t, Si_t, Fe_d and Fe_o) was determined as described in the SI for the bulk soil fraction (< 2 mm). Total organic carbon was determined with a Multi N/C 3100 total organic carbon (TOC) analyzer (Analytik Jena, Jena, Germany). All measurements were performed in triplicate. In reporting data, the bulk soil and NNP fractions are distinguished by "S" and "N" before each parameter (e.g., S-pH vs. N-pH).

Statistical analyses

Linear regressions between NNP stocks of the entire upper 1-m soil profile and chronosequence age were obtained using OriginPro 2016 software (OriginLab Corp., Northampton, MA, USA). Linear correlations between bulk soil (< 2 mm) and NNP properties were calculated using Pearson correlation coefficients (r) for the complete dataset (n = 25) with SPSS 16.0 (IBM Corp., USA). We performed a network analysis based on the Pearson correlation analysis between bulk soil and NNP properties using Gephi 0.9.2 (Bastian *et al.*, 2009).

We investigated relationships between bulk soil and NNP properties by multivariate analyses using CANOCO 5.0 and R-base packages. Canonical redundancy analysis (RDA) was used to test which bulk soil properties significantly explained the variation in NNP properties. All measured soil properties were $\log_{10}$-transformed (except pH) to improve normality and homoscedasticity for multivariate statistical analysis. Collinearity of bulk soil properties was investigated using variance inflation factors (VIF) and collinear variables with VIF > 20 were excluded. Significant variables for analysis were pre-selected from groups of variables (soil cultivation age, sand, silt, bulk density, pH, EC, CEC, ammonium acetate extractable K^+, Na^+, Mg^{2+}, total contents of Fe_t, Mn_t, Al_t, Si_t, Ti_t and Ti_t/Zr_t, Fe_d, Fe_o) by forward model selection. The significance of the RDA models and selected variables were determined by 999 Monte Carlo permutations at $P < 0.05$ for each group. The respective effects of variables or groups of variables on the variation in NNP properties were further investigated by canonical variation partitioning.

We assessed changes in bulk soil and NNP properties in different soil-age groups using hierarchical cluster analysis of standardized values for each soil layer. Principal component analysis (PCA) was applied to further explore similarities among age/depth groups based on NNP properties.

RESULTS

Characterization of natural nanoparticles

NNP content ranged from 0.2 to 6.2% of the bulk soil fraction (Table I). No NNPs were attained from the wetland soil (0-yr cultivation), which showed no evidence of soil horizon development based on field morphological investigations. NNP content was distinctly enriched in subsoil horizons of older soils (700−1000 yrs), but was more uniformly distributed with depth in younger soils (50−300 yrs) (Fig. 1a). Bulk soil properties (< 2-mm fraction) from the chronosequence are listed in Table SII and a detailed description of their variations across the chronosequence is presented in the SI. Compared to the clay contents of younger soils, the older soils had generally higher clay contents (Table SII). NNPs were all negatively charged based on zeta potential measurements and zeta potential significantly decreased with increasing cultivation age (r = –0.75, *P* < 0.01). The mineralogical composition of NNPs was constant and dominated by illite and montmorillonite, which

was consistent with the clay fraction (Fig. S2). A significant increase, at a rate of ~6.0 kg m^{-2} 100 yr^{-1}, of NNP stock in the 100-cm soil profile was found along the chronosequence (R^2 = 0.93; P < 0.01) (Fig. 2). The Fe$_d$ and TOC stocks within the NNP fraction increased linearly at rates of 0.21 and 0.08 kg m^{-2} 100 yr^{-1}, respectively. The stock of Fe$_t$, Fe$_o$ and Mn$_t$, within the NNP fraction also continuously accumulated with the increasing cultivation age. TEM images showed various NNP shapes consisting of irregular transparent and dark sheets (Fig. S3a, b). NNP size ranged from ~10 to ~100 nm, and the larger sizes were attributed to agglomeration of NNPs upon drying for TEM analysis. In comparison, the mean hydrodynamic size of NNPs in the upper topsoil (0−20 cm) varied from ~72 to ~89 nm and decreased with increasing cultivation age (Table I).

Correlations among bulk soil and NNP properties

Pearson correlations among bulk soil and NNP properties are provided in Fig. 3 and Supplementary Tables SIII and SIV. Soil cultivation age served as a keystone node in the correlation network, with a number of links to bulk soil and NNP properties (Fig. 3). Results indicated strong negative correlations between cultivation age and many bulk soil characteristics, including silt, EC, pH, extractable K$^+$, Na$^+$, and Ca^{2+} and S-Mn$_t$. Notably, clay content was positively correlated with cultivation age. Soil cultivation age was significantly correlated with NNP content, free Fe oxide (N-Fe$_d$) and crystalline Fe (N-Fe$_{do}$) (r = 0.878, 0.704 and 0.686, respectively), and they were positively correlated to each other (r ≥ 0.771). Soil cultivation age exhibited a significant negative relationship with NNP size, zeta potential and Mn$_t$ (r = –0.733, –0.750 and –0.701, respectively). Similarly, soil depth was significantly correlated with several bulk soil properties, including TOC, extractable K$^+$ and Mg^{2+}, Fe$_d$ and Fe$_{do}$, and with NNP TOC.

NNP content, N-Fe$_d$ and N-Fe$_{do}$ were negatively correlated with silt, EC and zeta potential, and positively related to clay, soil free Fe oxide (S-Fe$_d$) and crystalline Fe (S-Fe$_{do}$) (P < 0.01). N-TOC was significantly correlated with TOC of the bulk soil samples (r = 0.65, P < 0.01); N-TOC concentrations ranged from 8.7 to 37.6 g kg^{-1} and were higher in topsoil (0−40 cm) than subsoil (40−100 cm) horizons. N-TOC concentrations were higher than for bulk soil samples (3−20 g kg^{-1}; Table SII), indicating an accumulation of colloidal organic matter in the NNP fraction (Table I and Fig. 2).

As shown in Fig. 2, N-Fe$_d$ and N-Fe$_{do}$ continuously accumulated with increasing cultivation age. The distribution of N-Fe$_d$ content was significantly related to that of bulk soil samples (r = 0.69, P < 0.01) (Table SIII). The poorly crystalline Fe (N-Fe$_o$) content of NNPs was generally lower in subsoil horizons than in topsoil. However, in younger soils (50−300 yrs), N-Fe$_o$ showed an increase in the 80−100-cm depth (Table I). The N-Fe$_o$ was related to S-Fe$_o$ (r = 0.48, P < 0.05). The NNP crystalline Fe (N-Fe$_{do}$) fraction also increased in deeper horizons after long-term paddy management and was correlated to S-Fe$_{do}$ (r = 0.78, P < 0.01). As shown in Fig. 1c, total Mn (N-Mn$_t$) content of NNPs decreased in older soils (700−1000 yrs) and was correlated to S-Mn$_t$ (r = 0.67, P < 0.01). Minimal changes were observed in N-Al$_t$ and N-Si$_t$ contents.

To further determine the key bulk soil properties controlling changes in NNP properties, we employed RDA to quantify the role of bulk soil properties. Significant factors were soil cultivation age, bulk density, and extractable K$^+$ and Mg^{2+}. For the first two main axes, the RDA explained 68.9% and 7.4% of the variation in NNP properties, with the selected bulk soil properties accounting for 79.1% of this variance. The major portion of the variance was explained by soil cultivation age and extractable K$^+$ on the first RDA axis 1, among which 60.7% of the variation was explained by soil cultivation age. Axis 2 was mainly related to soil bulk density and extractable Mg^{2+}.

Classification of age/depth groups based on NNP properties

Selected NNP properties were used to conduct the hierarchical cluster analysis. Findings showed that samples were split into 50−300-yr and 700−1000-yr age groups in all soil layers (Fig. S4), which was different from the classification based on bulk soil properties. Details about classification of age/depth groups based on bulk soil properties are presented in the SI. Specifically, the older soils (700−1000 yrs) tended to show higher clay and NNP contents, accompanied by lower EC, pH and zeta potential values. Higher TOC contents were always found in the upper topsoil (0−20 cm), while higher clay, S-Fe$_d$ and N-Fe$_d$ were found at deeper depths in older soils (700−1000 yrs).

PCA analysis was applied to further discriminate age/depth groups of NNP properties. The score plot (Fig. S5) revealed that the first two principal components represented 78.2% and 10.5% of the total variance. The cumulative contribution rate of the first two PCs was 88.7%, which extensively describes the age/depth groups of the NNP samples. The NNP samples were clearly split into 50−300-yr and 700−1000-yr age groups (Fig. S5).

DISCUSSION

NNP distribution in the soil chronosequence

Across the chronosequence, a longer cultivation age resulted in an increase of NNPs (Fig. 1a and Fig. 2), especially in subsoil horizons (40−100-cm depth). NNPs shared a similar distribution trend to that of clay (r = 0.83, P < 0.01), which is consistent with previously reported correlations between the contents of water-dispersible colloids and total clay (Vendelboe *et al.*, 2012). Both NNP and clay fractions were strongly correlated with cultivation age (r = 0.88 and 0.68, respectively). Translocation of fine particles by dispersion and illuviation could influence the vertical distribution of NNPs in soils with increasing cultivation age. Downward translocation of soil particles in paddy soils maybe attributed to pedogenic processes induced by long-term human activities, such as plowing, drainage and flooding (Zhang and Gong, 2003).

Additional pedogenic processes associated with the redistribution of NNPs at the soil profile scale may result from human-induced changes in EC and zeta potentials. Soil EC showed a negative correlation with cultivation age (r = −0.77, P < 0.01) and NNP content (r = −0.53, P < 0.01). Similarly, zeta potential values for NNPs were strongly correlated with soil EC (r = 0.80, P <0.01). Jiang *et al.* (2017) demonstrated with soil column experiments that NNP dispersion and transport were strongly enhanced in lower ionic strength solutions that also involved a decrease in NNP zeta potentials. Concomitant with the decrease in EC, extractable K^+, Na^+ and Ca^{2+} decreased with time since the start of cultivation (r = −0.54, −0.56 and −0.80, respectively). These results suggest that the formation and redistribution of NNPs were strongly influenced by desalination and decalcification.

Previous studies of soil colloids indicated that a decrease of ionic strength could favor colloid mobilization in water-saturated columns (Zhang and Selim, 2007; Zhou *et al.*, 2011). The sensitivity of colloidal dispersion to monovalent (Na^+ enhances dispersion) versus divalent cations (Ca^{2+} promotes flocculation) also contributes to flocculation/dispersion dynamics (Shainberg *et al.*, 1981). High electrolyte concentrations (*i.e.*, high EC) decrease the thickness of the diffuse double layer of NNPs leading to coagulation by enhanced van der Waals attraction (Li *et al.*, 2016). When electrolyte concentrations increase, the absolute values of zeta potentials become less than 30 mV (which is considered a threshold for NNP aggregate stability) resulting in a decrease in electrostatic repulsion (Zhu *et al.*, 2014). As a result, illite and montmorillonite were susceptible to high electrolyte and Ca^{2+} concentrations in the younger soils that promoted aggregation (Tombacz and Szekeres, 2004).

Similarly, ionic strength could influence the heterocoagulation of iron oxides and other mineral particles (Sotirelis and Chrysikopoulos, 2017), which was also reflected in the relationship between iron oxides and NNPs in our study.

Before cultivation-induced desalinization/decalcification, high electrolyte concentrations maintained absolute values for NNP zeta potentials of less than 30 mV resulting in formation of stable NNP aggregates, which limited the content of NNPs in the chronosequence. Accordingly, the wetland sample (0-yr cultivation) had negligible extractable NNPs after ultrasonic treatment, in part due to the effects of high EC and Ca^{2+} contents on formation of stable NNP aggregates. As cultivation age increased and desalinization/decalcification progressed, the decrease of ionic strength and Ca^{2+} contents increased the repulsive forces between mineral surfaces promoting dispersion of NNP aggregates, which also contributed to decreased NNP size with increasing cultivation age (Miao et $al.$, 2015). In addition, natural organic matter can enhance the water stability of NPs, in which electrostatic repulsion plays an important role in interactions of NPs (Zhu et $al.$, 2017). This may partially explain the increase in NNPs as the TOC content of the NNP fraction increased during development in the soil chronosequence (Fig. 1b).

Results from Wissing et $al.$ (2013) demonstrated that Fe oxides strongly interacted with TOC in soil and promoted accumulation of TOC during paddy cultivation. Since $N-Fe_o$ was related to N-TOC (r = 0.339, Table SIV), the higher Fe_o proportion in NNPs induced by long-term paddy soil management (Fig. 2e) could similarly accelerate the accumulation of N-TOC. Additionally, TOC accumulation could impart highly negative zeta potentials to NNPs, which increases electrostatic repulsive forces between NNPs, thereby reducing their aggregation, as well as forming smaller and more stable NNPs (Miao et $al.$, 2015; Li et $al.$, 2016; Wang et $al.$, 2019) with prolonged rice cultivation. As a result, NNP aggregates were dispersed as individual NNPs contributing to the translocation and accumulation of NNPs predominantly in subsoil horizons of the older (700−1000 yrs) soils (Fig. 1a). Therefore, the changes in NNP content and profile distribution were appreciably influenced by human-induced changes in EC and zeta potential during development of the soil chronosequence.

Changes of NNP properties across the soil chronosequence

Despite many years of paddy cultivation, NNP Al_t and Si_t contents did not significantly change across the chronosequence (Table I). This is consistent with our previous research that indicated the composition of NNPs was directly related to the properties of the parent material from which the soils were derived (Li et $al.$, 2012). Chen et $al.$ (2011) reported that 1000 years of paddy cultivation caused only small changes to aluminosilicate clay minerals. We found no clear trend for changes in the elemental composition of either the bulk soil or NNP fraction across the 1000-year-old chronosequence (Tables SII and SIII).

In contrast to elemental composition, some NNP properties changed significantly during the 1000 years of paddy cultivation. RDA analysis demonstrated that soil cultivation age alone could explain up to 60.7% of the temporal variation in NNP properties (Fig. 4). TOC, Fe_d, Fe_o, Fe_{do} and Mn_t contents in the NNP fraction were positively correlated with those of the bulk soil (Fig. 3 and Table SIII). Among these properties, changes in Fe fractions were particularly evident and illustrated active chemical weathering and pedogenesis (Fig. 1). Both $N-Fe_d$ and $N-Fe_o$ accumulated in older paddy soils (700−1000 yrs) and increased with increasing cultivation age (Table I and Fig. 2). Further, $N-Fe_{do}$ (*i.e.,* crystalline Fe oxide fraction of NNPs) was positively related with $N-Fe_d$ (r = 0.91) and comprised the majority of $N-Fe_d$ in subsoil horizons of older paddy soils (700−1000 yrs). Our results

demonstrated a stronger relationship between the Fe_{do} concentration of NNPs and cultivation age (r = 0.69) than that of the bulk soil (r = 0.37) (Table SIII). The Fe_{do} fraction might interact with the microbial community by restraining the availability of substrate owing to organic matter sorption onto iron minerals (Dippold *et al.*, 2014; Turner *et al.*, 2019). Thus, N-Fe_{do} may play an important role due to its large increase with cultivation age and greater mobility (Liu *et al.*, 2018). Redox cycles in paddy soils could lead to a higher proportion of Fe_o oxides (poorly crystalline forms) (Wissing *et al.*, 2014). Wissing *et al.* (2013) reported a higher proportion of poorly crystalline Fe present after about 50 years of paddy soil management. The N-Fe distribution suggested that redox processes were similarly affecting all Fe fractions. In addition, N-Mn content decreased with the increasing cultivation age (r = −0.70) (Table SIII). The more dynamic redox nature of Mn makes it more mobile than Fe under reducing conditions explaining the preferential loss of Mn from paddy soils (Huang *et al.*, 2017). Eluviation of Mn began at the early stages of paddy management, and commenced much earlier than the increase of Fe_d in subsoil horizons.

As for the organic matter properties of NNPs, N-TOC accumulated in the upper topsoil (0−20 cm) (Fig. 1b) and its concentrations were negatively correlated with soil depth (r = −0.70). Pearson correlation analysis indicated that the NNP organic matter properties were similar to those of the bulk soil across the chronosequence. Paddy management has been shown to slow decomposition rates and favor the accumulation of soil organic matter (Sahrawat, 2004), and its accumulation was demonstrated in topsoil horizons for the entire period of paddy development (Kolbl *et al.*, 2014; Wissing *et al.*, 2014). After 50 years of cultivation, the differences in soil organic carbon between topsoil and subsoil horizons became more evident (Chen *et al.*, 2011). There was evidence for a more rapid increase of N-TOC in the upper topsoil (0−20 cm) within 50−300 yrs relative to N-TOC accumulation over 700−1000 yrs (Fig. 1). In contrast, N-TOC concentrations in subsoil horizons changed only slightly throughout the entire soil chronosequence.

Implications of natural nanoparticles

The effects of long-term paddy management to recently reclaimed coastal soils were evident for bulk soil and NNP properties across the 1000-year soil chronosequence. Categorization of pedogenic processes by cluster and PCA analyses (Figs. S4 and S5) divided the cumulative pedogenic processes into two periods. Cluster analysis for NNPs divided all soil layers of the chronosequence into T1 (50−300 yrs) and T2 (700−1000 yrs) periods. By contrast, based on bulk soil, the T1 period included the 50−100-yrs topsoil samples (0−40 cm) and the 50−700-yrs subsoil samples (40−100 cm, while the T2 period included the 100−1000-yrs topsoil samples (0−40 cm) and the 700−1000-yrs subsoil samples (40−100 cm) (Fig. S6). The difference between the two categorizations was due to a delayed response in changes of NNP properties relative to the bulk soil.

Desalinization and decalcification are common phenomena that take place in land reclamation of coastal regions (Wissing *et al.*, 2014). The high EC and Ca^{2+} contents during the initial reclamation period lead to a low NNP content, likely due to the formation of water-stable aggregates composed of NNPs. After the initial process of desalinization/decalcification within ~50 years, eluviation of Mn and accumulation of TOC in the upper topsoil (0−20 cm) were observed in the NNP fraction. As EC and pH values continuously decreased during this period, NNP accumulation was initiated, which extended through the first stage (T1) of pedogenesis (50−300 years). During the second stage (T2), EC and pH values reached a steady-state, which allowed for dispersion of NNP aggregates leading to a relatively continuous increase in NNP content (6.0 kg m^{-2} 100 yr^{-1}) over the study period. In addition, Fe_o and TOC preferentially increased in the upper topsoil (0−20 cm) during this period. The

accumulation of N-TOC owing to association with N-Fe$_o$ could be terminated by leaching of Fe oxide (Wissing *et al.*, 2013). However, it did not occur even after 1000 years of paddy management. The results indicated that novel paddy soil management procedures (e.g., alternating wetting and drying) should be addressed in subsequent research, because paddy management alters redox conditions, as well as the Fe oxide composition and its potential for organic carbon storage. Iron oxide accumulation and increased crystallization were evident in deeper subsoil horizons (40−100 cm) for both the NNP and bulk soil fractions. The change of NNP properties were related to changes in the bulk soil properties. Following changes in bulk soil properties, the changes in NNP properties were delayed, and thus the cluster analysis based on NNP properties divided pedogenesis into two distinct periods (50−300 years and 700−1000 years) in all soil layers. Given the significant impacts of paddy soils in global biogeochemical cycles and food production, appropriate water management to realize optimal EC, pH and redox conditions in paddy soils during their millennial-scale evolution needs more attention.

CONCLUSIONS

Our investigation represents a first attempt to track NNP evolution during pedogenesis along a long-term paddy soil chronosequence. We demonstrated that the distribution and properties of NNPs were strongly affected by long-term soil management in a chronosequence spanning the range of 0−1000 years. Some NNP properties, such as Fe and TOC contents and NNP profile distribution, changed considerably with increasing cultivation age and were in an agreement with bulk soil properties as hypothesized. Long-term paddy management-initiated desalinization/decalcification, chemical weathering (especially Mn/Fe redox transformations) and pedogenesis that may subsequently impact microbial communities and contaminant transport. Network and redundancy analyses indicated that soil cultivation age was the predominant factor affecting NNP properties, with a contribution of 60.7% of the total variability. In contrast, soil depth was not a dominant factor controlling variations in NNP properties. Overall, this study provides valuable insights into understanding how NNPs change over long-time periods and may be used to predict how NNP evolution over time might impact agricultural productivity and pollutant fate/transport. Future studies should cover a broader spectrum of soil types, looking for idiosyncrasies and commonalities, in an effort to create a holistic view of NNP evolution in soil environments.

ACKNOWLEDGMENTS

SUPPLEMENTARY MATERIAL

Supplementary material for this article is available in the online version.

REFERENCES

Bakshi S, He Z, Harris W G. 2014. A new method for separation, characterization, and quantification of natural nanoparticles from soils. *J Nanopart Res*. **16:** 2261−2271.

Bakshi S, He Z L, Harris W G. 2015. Natural nanoparticles: Implications for environment and human health. *Crit Rev Env Sci Tec*. **45:** 861-904.

Bastian M, Heymann S, Jacomy M. 2009. Gephi: An open source software for exploring and manipulating networks. In Third international AAAI conference on weblogs and social media.

Chen L, Zhang G, Effland W R. 2011. Soil characteristic response times and pedogenic thresholds during the 1000-year evolution of a paddy soil chronosequence. *Soil Sci Soc Am J*. **75:** 1807-1820.

Dippold M, Biryukov M, Kuzyakov Y. 2014. Sorption affects amino acid pathways in soil: Implications from position-specific labeling of alanine. *Soil Biol Biochem*. **72:** 180-192.

Guo Y, Wu X, Pan C, Zhang J. 2012. Numerical simulation of the tidal flow and suspended sediment transport in the Qiantang estuary. *J Waterw Port Coast*. **138:** 192-202.

Han G, Zhang G, Li D, Yang J. 2015. Pedogenetic evolution of clay minerals and agricultural implications in three paddy soil chronosequences of south China derived from different parent materials. *J Soil Sediment*. **15:** 423-435.

Hochella M F, Lower S K, Maurice P A, Penn R L, Sahai N, Sparks D L, Twining B S. 2008. Nanominerals, mineral nanoparticles, and earth systems. *Science*. **319:** 1631-1635.

Hochella M F, Mogk D W, Ranville J, Allen I C, Luther G W, Marr L C, McGrail B P, Murayama M, Qafoku N P, Rosso K M, Sahai N, Schroeder P A, Vikesland P, Westerhoff P, Yang Y. 2019. Natural, incidental, and engineered nanomaterials and their impacts on the Earth system. *Science. (80-)* **363**:eaau8299.

Hochella M F, Spencer M G, Jones K L. 2015. Nanotechnology: Nature's gift or scientists' brainchild? *Environ Sci Nano*. **2:** 114-119.

Huang L, Thompson A, Zhang G, Chen L, Han G, Gong Z. 2015. The use of chronosequences in studies of paddy soil evolution: A review. *Geoderma*. **237-238:** 199-210.

Huang Q, Tang S, Huang X, Zhang F, Yi Q, Li P, Fu H. 2017. Influence of rice cultivation on the abundance and fractionation of Fe, Mn, Zn, Cu, and Al in acid sulfate paddy soils in the Pearl River Delta. *Chem Geol*. **448**:93–99.

Jiang J, Dai Z, Sun R, Zhao Z, Dong Y, Hong Z, Xu R. 2017. Evaluation of ferrolysis in arsenate adsorption on the paddy soil derived from an Oxisol. *Chemosphere*. **179:** 232-241.

Jiang Y, Yu L, Sun H, Yin X, Wang C, Mathews S, Wang N. 2017. Transport of natural soil nanoparticles in saturated porous media: Effects of pH and ionic strength. *Chem Spec Bioavail*. **29:** 186-196.

Koelbl A, Schad P, Jahn R, Amelung W, Bannert A, Cao Z H, Fiedler S, Kalbitz K, Lehndorff E, Mueller-Niggemann C, Schloter M, Schwark L, Vogelsang V, Wissing L, Koegel-Knabner I. 2014. Accelerated soil formation due to paddy management on marshlands (Zhejiang Province, China). *Geoderma*. **228:** 67-89.

Leff B, Ramankutty N, Foley J A. 2004. Geographic distribution of major crops across the world. *Global Biogeochem Cycles*. **18**.

Li S, Ma H, Wallis L K, Etterson M A, Riley B, Hoff D J, Diamond S A. 2016. Impact of natural organic matter on particle behavior and phototoxicity of titanium dioxide nanoparticles. *Sci Total Environ*. **542**:324–333.

Li W, He Y, Wu J, Xu J. 2012. Extraction and characterization of natural soil nanoparticles from Chinese soils. *Eur J Soil Sci*. **63:** 754-761.

Liu F, Xu B, He Y, Brookes P C, Xu J. 2019a. Co-transport of phenanthrene and pentachlorophenol by natural soil nanoparticles through saturated sand columns. *Environ Pollut*. **249:** 406-413.

Liu G, Ma J, Yang Y, Yu H, Zhang G, Xu H. 2019b. Effects of straw incorporation methods on nitrous oxide and methane emissions from a wheat-rice rotation system. *Pedosphere*. **29:** 204-215.

Liu Y, Dong Y, Wang P, Hussain Q, Ge T, Wang J. 2019c. Distribution of methane production and methanogenic archaeal community structure across soil particle size fractions along a rice chronosequence. *J Soil Water Conserv.* **74**:235–246.

Liu F, Xu B, He Y, Brookes P C, Tang C, Xu J. 2018. Differences in transport behavior of natural soil colloids of contrasting sizes from nanometer to micron and the environmental implications. *Sci Total Environ.* **634:** 802-810.

Miao L, Wang C, Hou J, Wang P, Ao Y, Dai S, Lv B. 2015. Effects of pH and natural organic matter (NOM) on the adsorptive removal of CuO nanoparticles by periphyton. *Environ Sci Pollut Res.* **22**:7696–7704.

Qian H, Huang S, Chen J, Wang L, Hungate B A, van Kessel C, Zhang J, Deng A, Jiang Y, van Groenigen KJ, Zhang W. 2020. Lower-than-expected CH_4 emissions from rice paddies with rising CO_2 concentrations. *Glob Chang Biol.* **26**:2368–2376.

Rod K, Um W, Chun J, Wu N, Yin X, Wang G, Neeves K. 2018. Effect of chemical and physical heterogeneities on colloid-facilitated cesium transport. *J Contam Hydrol.* **213**:22–27.

Shainberg I, Rhoades J D, Prather R J. 1981. Effect of low electrolyte concentration on clay dispersion and hydraulic conductivity of a sodic soil. *Soil Sci Soc Am J.* **45:** 273-277.

Soil Survey Staff. 2014. Keys to Soil Taxonomy. 12th ed. U.S. Department of Agriculture, Natural Resources Conservation Service, Washington, DC.

Song Y, Bian Y, Wang F, Herzberger A, Yang X, Gu C, Jiang X. 2017. Effects of biochar on dechlorination of hexachlorobenzene and the bacterial community in paddy soil. *Chemosphere* **186:** 116-123.

Sotirelis NP, Chrysikopoulos C V. 2017. Heteroaggregation of graphene oxide nanoparticles and kaolinite colloids. *Sci Total Environ.* **579**:736–744.

Taghipour M, Jalali M. 2018. Heavy metal release from some industrial wastes: Influence of organic and inorganic acids, clay minerals, and nanoparticles. *Pedosphere.* **28:** 70-83.

Theng B K G, Yuan G. 2008. Nanoparticles in the soil environment. *Elements.* **4**: 395–399.

Tombacz E, Szekeres M. 2004. Colloidal behavior of aqueous montmorillonite suspensions: The specific role of pH in the presence of indifferent electrolytes. *Appl Clay Sci.* **27:** 75-94.

Turner S, Mikutta R, Guggenberger G, Schaarschmidt F, Schippers A. 2019. Distinct pattern of nitrogen functional gene abundances in top- and subsoils along a 120,000-year ecosystem development gradient. *Soil Biol Biochem.* **132:** 111-119.

Van Den Bogaert R, Labille J, Cornu S. 2015. Aggregation and dispersion behavior in the 0-to 2-μm fraction of Luvisols. *Soil Sci Soc Am J.* **79:** 43-54.

Vendelboe A L, Moldrup P, Schjonning P, Oyedele D J, Jin Y, Scow K M, de Jonge L W. 2012. Colloid release from soil aggregates: Application of laser diffraction. *Vadose Zone J.* **11**.

Wang X, Wang S, Pan X, Gadd GM. 2019. Heteroaggregation of soil particulate organic matter and biogenic selenium nanoparticles for remediation of elemental mercury contamination. *Chemosphere.* **221:** 486-492.

Watanabe T, Asakawa S, Hayano K. 2020. Long-term submergence of non-methanogenic oxic upland field soils helps to develop the methanogenic archaeal community as revealed by pot and field experiments. *Pedosphere.* **30:** 62-72.

Wei C, Gao W, Whalley W R, Li B. 2018. Shrinkage characteristics of lime concretion black soil as affected by biochar amendment. *Pedosphere.* **28:** 713-725.

Wissing L, Koelbl A, Häusler W, Schad P, Cao Z, Koegel-Knabner I. 2013. Management-induced organic carbon accumulation in paddy soils: The role of organo-mineral associations. *Soil Tillage Res.* **126**: 60–71.

Wissing L, Koelbl A, Schad P, Braeuer T, Cao Z, Koegel-Knabner I. 2014. Organic carbon accumulation on soil mineral surfaces in paddy soils derived from tidal wetlands. *Geoderma.* **228**: 90-103.

Xie D, Pan C, Wu X, Gao S, Wang Z B. 2017. Local human activities overwhelm decreased sediment supply from the Changjiang River: Continued rapid accumulation in the Hangzhou Bay-Qiantang Estuary system. *Mar Geol*. **392:** 66-77.

Xie D, Wang Z, Gao S, De Vriend H J. 2009. Modeling the tidal channel morphodynamics in a macro-tidal embayment, Hangzhou Bay, China. *Cont Shelf Res*. **29:** 1757-1767.

Xu B, Lian Z, Liu F, Yu Y, He Y, Brookes P C, Xu J. 2019. Sorption of pentachlorophenol and phenanthrene by humic acid coated hematite nanoparticles. *Environ Pollut*. **248:** 929-937.

Zhang G L, Gong Z T. 2003. Pedogenic evolution of paddy soils in different soil landscapes. *Geoderma.* **115:** 15-29.

Zhang H, Selim H M. 2007. Colloid mobilization and arsenite transport in soil columns: Effect of ionic strength. *J Environ Qual*. **36:** 1273-1280.

Zhang W, Tang X Y, Xian Q S, Weisbrod N, Yang J E, Wang H L. 2016. A field study of colloid transport in surface and subsurface flows. *J Hydrol.* **542**:101–114.

Zhou D, Wang D, Cang L, Hao X, Chu L. 2011. Transport and re-entrainment of soil colloids in saturated packed column: Effects of pH and ionic strength. *J Soil Sediment*. **11:** 491-503.

Zhou H, Fang H, Mooney S J, Peng X. 2016. Effects of long-term inorganic and organic fertilizations on the soil micro and macro structures of rice paddies. *Geoderma.* **266:** 66-74.

Zhu X, Chen H, Li W, He Y, Brookes P C, Xu J. 2014. Aggregation kinetics of natural soil nanoparticles in different electrolytes. *Eur J Soil Sci*. **65:** 206-217.

Zhu X, Chen H, Li W, He Y, Brookes PC, White R, Xu J. 2017. Evaluation of the stability of soil nanoparticles: The effect of natural organic matter in electrolyte solutions. *Eur J Soil Sci*. **68:** 105-114.

Zhu Z, Ge T, Liu S, Hu Y, Ye R, Xiao M, Tong C, Kuzyakov Y, Wu J. 2018. Rice rhizodeposits affect organic matter priming in paddy soil: The role of N fertilization and plant growth for enzyme activities, CO_2 and CH_4 emissions. *Soil Biol Biochem.* **116**:369–377.

1   TABLE I Properties of nanoparticles extracted from soil samples in Cixi chronosequence (mean ± SD, n = 3).

Age years	Soil depth cm	Mean size (Intensity) nm	Nanoparticle content %	Zeta Potential mV	TOC $g\ kg^{-1}$	Fe_t $g\ kg^{-1}$	Fe_d $g\ kg^{-1}$	Fe_o $g\ kg^{-1}$	Mn_t $g\ kg^{-1}$	Al_t $g\ kg^{-1}$	Si_t $g\ kg^{-1}$
50	0−20	84 ± 10	0.3 ± 0.1	-23 ± 1	35 ± 6	74 ± 3	22 ± 4	18 ± 5	1.14 ± 0.09	105 ± 3	194 ± 7
50	20−40	87 ± 2	0.2 ± 0.1	-23 ± 1	31 ± 5	65 ± 3	13 ± 2	8 ± 2	1.43 ± 0.16	105 ± 4	208 ± 8
50	40−60	97 ± 13	0.5 ± 0.2	-25 ± 1	21 ± 4	87 ± 4	24 ± 3	13 ± 2	1.41 ± 0.12	111 ± 4	201 ± 8
50	60−80	97 ± 14	0.3 ± 0.1	-24 ± 1	13 ± 3	74 ± 1	21 ± 5	9 ± 3	0.90 ± 0.13	109 ± 4	211 ± 10
50	80−100	91 ± 25	0.9 ± 0.3	-25 ± 1	17 ± 4	71 ± 7	36 ± 6	12.6 ± 3	0.71 ± 0.12	104 ± 6	218 ± 5
100	0−20	89 ± 12	1.9 ± 0.6	-22 ± 0	32 ± 5	72 ± 3	18 ± 3	15 ± 3	1.20 ± 0.05	110 ± 2	205 ± 15
100	20−40	91 ± 20	0.3 ± 0.1	-25 ± 3	25 ± 5	56 ± 4	15 ± 4	7 ± 1	1.00 ± 0.13	107 ± 3	228 ± 8
100	40−60	95 ± 14	0.8 ± 0.2	-23 ± 3	22 ± 2	60 ± 5	22 ± 2	13 ± 3	0.77 ± 0.06	106 ± 3	207 ± 8
100	60−80	97 ± 8	0.6 ± 0.2	-22 ± 0	15 ± 3	87 ± 3	24 ± 3	16 ± 4	1.24 ± 0.10	103 ± 4	182 ± 9
100	80−100	82 ±10	1.1 ± 0.3	-23 ± 1	18 ± 2	69 ± 4	31 ± 3	18 ± 5	1.05 ± 0.08	104 ± 3	204 ± 10
300	0−20	82 ± 8	1.6 ± 0.4	-29 ± 4	38 ± 2	91 ± 4	28 ± 3	15 ± 4	0.77 ± 0.15	107 ± 5	218 ± 10
300	20−40	81 ± 10	0.5 ± 0.1	-29 ± 3	25 ± 5	70 ± 6	21 ± 5	15 ± 5	0.65 ± 0.07	105 ± 3	199 ± 12
300	40−60	89 ± 3	1.5 ± 0.0	-28 ± 4	14 ± 4	67 ± 5	31 ± 2	12 ± 1	0.48 ± 0.07	99 ± 4	222 ± 8
300	60−80	88 ± 7	1.1 ± 0.2	-25 ± 1	9 ± 2	80 ± 5	30 ± 3	17 ± 1	0.68 ± 0.04	103 ± 4	194 ± 11
300	80−100	87 ± 15	2.0 ± 0.3	-24 ± 0	14 ± 3	94 ± 3	34 ± 5	20 ± 6	1.04 ± 0.06	104 ± 2	238 ± 6
700	0−20	80 ± 14	3.0 ± 0.9	-22 ± 0	22 ± 6	88 ± 2	34 ± 6	17 ± 5	0.57 ± 0.02	104 ± 4	210 ± 13
700	20−40	77 ± 22	2.3 ± 0.6	-29 ± 1	14 ± 3	76 ± 4	31 ± 5	12 ± 2	0.84 ± 0.02	107 ± 3	224 ± 10
700	40−60	89 ± 14	5.0 ± 1.2	-31 ± 3	9 ± 1	96 ± 3	41 ± 7	7 ± 1	0.49 ± 0.06	106 ± 2	219 ± 9
700	60−80	79 ± 17	5.6 ± 1.4	-31 ± 3	9 ± 1	104 ± 2	38 ± 6	6 ± 1	0.52 ± 0.06	113 ± 3	224 ± 6
700	80−100	84 ± 12	2.7 ± 0.6	-36 ± 5	13 ± 3	73 ± 4	46 ± 5	11 ± 3	0.56 ± 0.05	106 ± 3	217 ± 9
1000	0−20	72 ± 13	2.5 ± 0.5	-31 ± 4	26 ± 5	79 ± 4	32 ± 7	23 ± 5	0.80 ± 0.11	105 ± 3	184 ± 8
1000	20−40	81 ± 11	4.3 ± 1.3	-31 ± 5	14 ± 2	58 ± 2	27 ± 6	9 ± 2	0.60 ± 0.07	106 ± 3	196 ± 12
1000	40−60	75 ± 10	5.9 ± 1.4	-30 ± 4	10 ± 2	88 ± 2	45 ± 5	7 ± 1	0.52 ± 0.05	103 ± 4	194 ± 8
1000	60−80	84 ± 7	6.2 ± 1.6	-30 ± 3	9 ± 1	101 ± 3	45 ± 4	10 ± 2	0.49 ± 0.02	100 ± 3	206 ± 13
1000	80−100	79 ± 12	5.3 ± 0.7	-30 ± 4	16 ± 4	92 ± 3	39 ± 3	9 ± 2	0.47 ± 0.03	101 ± 2	195 ± 6

2   Fe_t = total Fe; Fe_d = crystalline + poorly crystalline Fe; Fe_o = poorly crystalline Fe.
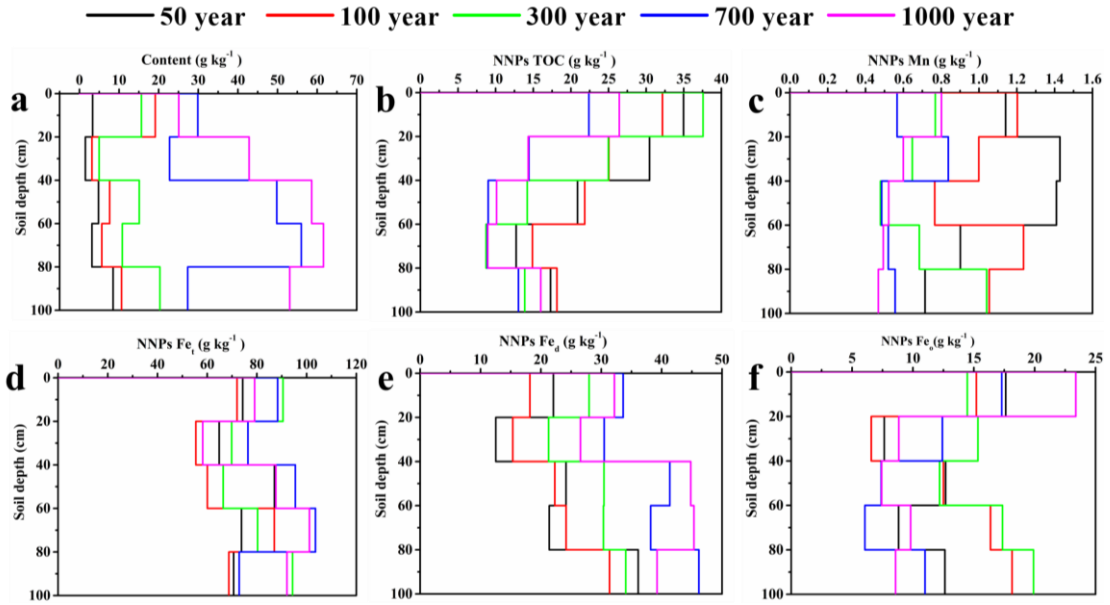
Fig. 1 Vertical distribution of natural nanoparticles (NNPs) (a), TOC (b), total Mn (c), total Fe (d), crystalline Fe oxide (e) and poorly crystalline Fe (f) fraction of NNPs across the soil chronosequence.

7
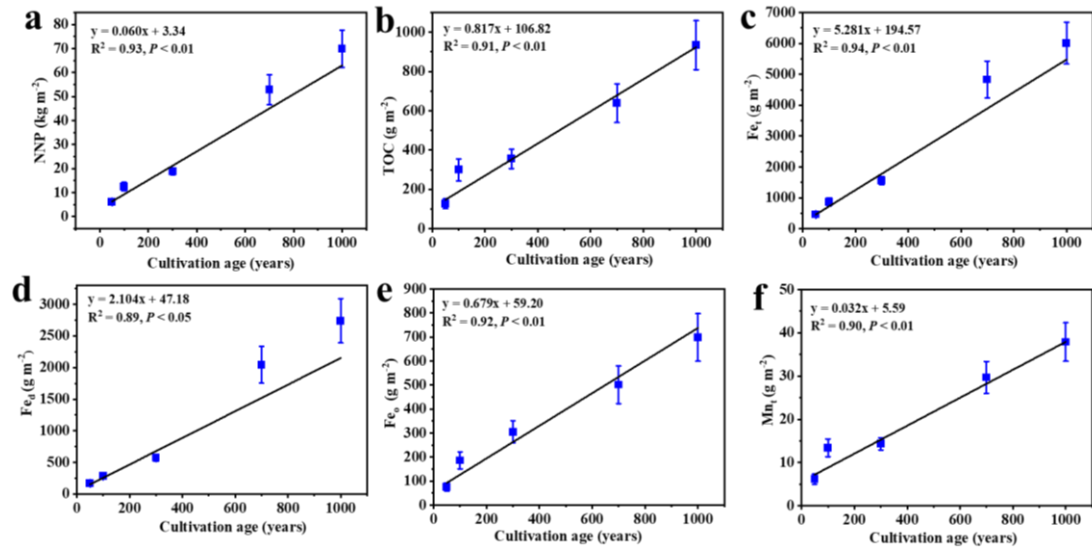
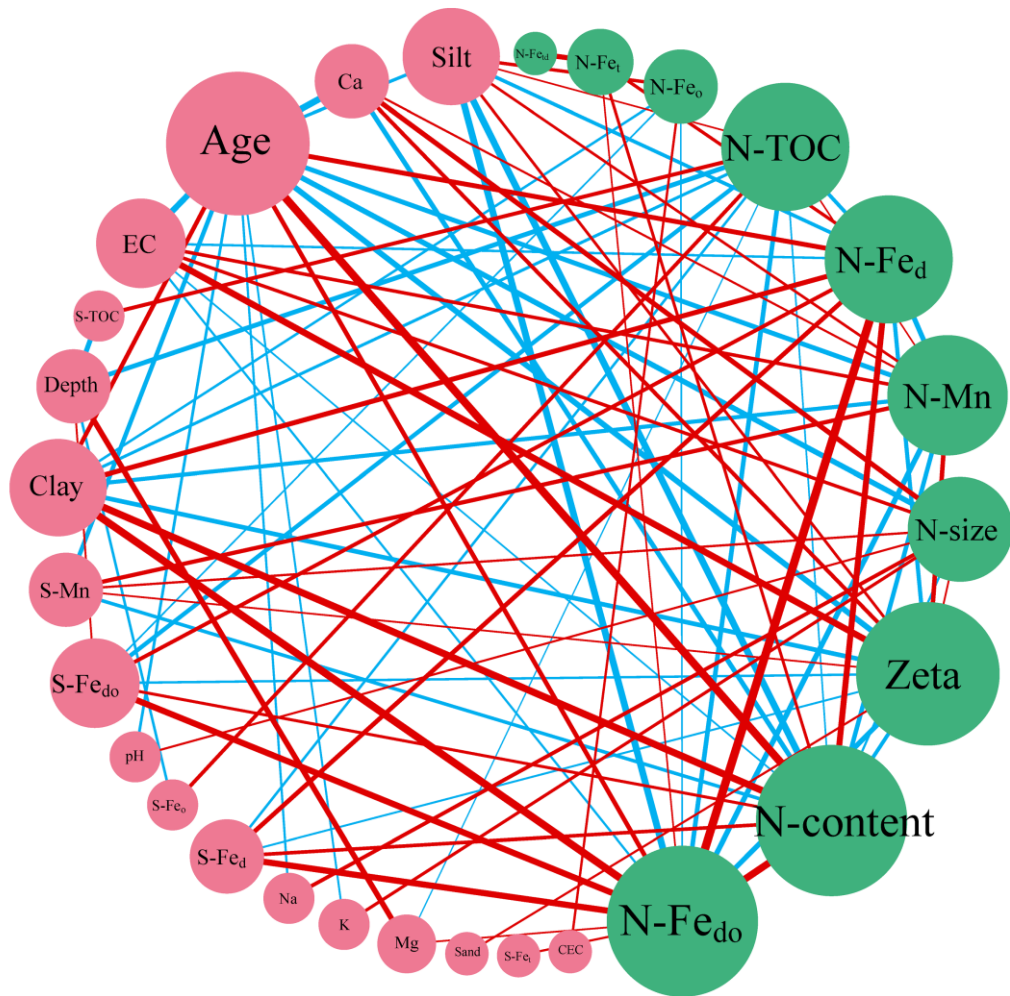Fig. 2 Linear correlations between cultivation age and NNP (a), TOC (b), Fe_t (c), Fe_d (d),

Fe$_o$ (e) and Mn$_t$ (f) stocks, respectively, for the 1-m soil profile along Cixi

chronosequence. Fe_t = total Fe; Fe_d = crystalline and poorly crystalline Fe; Fe_o = poorly

crystalline Fe; Mn_t = total Mn.

12

Fig. 3 Associations between bulk soil (pink) and NNP properties (green) visualized as

a network. Only Pearson's correlations at the Bonferroni-corrected level of $P < 0.01$ are

depicted. Pearson correlation coefficients are indicated by line width. Positive linkages

are shown in red, while negative linkages are shown in blue. Node sizes are proportional

to the number of correlations. For a complete list of correlation values see

Supplementary Tables SIII and SIV.

19
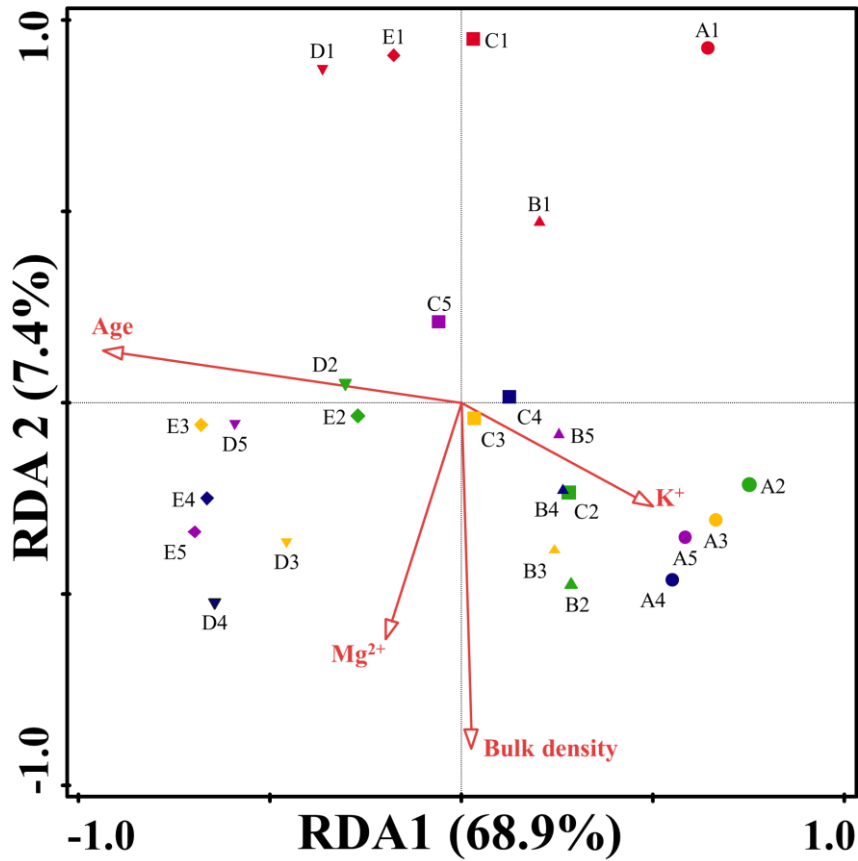
Fig. 4 Redundancy analysis (RDA) plot of bulk soil and NNP properties. Letters next

to the symbols indicate the cultivation age 50 (A), 100 (B), 300 (C), 700 (D) and 1000

(E). Numbers associated with the letters correspond to sampling depth 0−20 cm (1),

20−40 cm (2), 40−60 cm (3), 60−80 cm (4) and 80−100 cm (5). Different symbols

and colors are used to distinguish samples of different cultivation age and depths.

Only bulk soil properties that significantly explained variability in NNP properties in

the forward selection procedure were fitted to the ordination (red arrows).